Journal of Medicinal Chemistry

Article

pubs.acs.org/jmc

Syntheses of 2-Nitroimidazole Derivatives Conjugated with 1,4,7-Triazacyclononane-*N*,*N*′-Diacetic Acid Labeled with F-18 Using an Aluminum Complex Method for Hypoxia Imaging

Lathika Hoigebazar,[†,‡] Jae Min Jeong,*[,†,‡] Ji-Youn Lee,[†,‡] Dinesh Shetty,[†,‡] Bo Yeun Yang,[†,‡] Yun-Sang Lee,[†,‡] Dong Soo Lee,[†,‡] June-Key Chung,[†,‡] and Myung Chul Lee[†,‡]

[†]Radiation Applied Life Sciences, Department of Nuclear Medicine, Institute of Radiation Medicine, Seoul National University College of Medicine, Seoul 110-744, Korea

[‡]Cancer Research Institute, Seoul National University College of Medicine, Seoul 110-744, Korea

Supporting Information

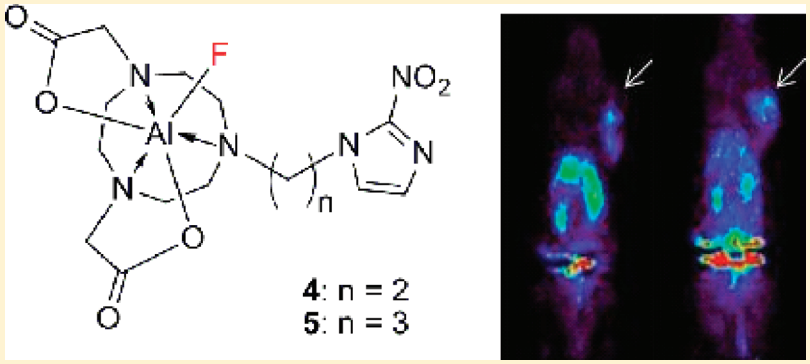

ABSTRACT: Hypoxia imaging is important for diagnosis of ischemic diseases, and thus various ^{18}F-labeled radiopharmaceuticals have been developed. However, ^{18}F-labeling requires multistep procedures including azeotropic distillation, which is complicated and difficult to automate. Recently, ^{18}F-labeling method using Al−F complex in aqueous solution was devised that offered a straightforward ^{18}F-labeling procedure. We synthesized nitroimidazole derivatives conjugated with 1,4,7-triazacyclononane-1,4-diacetic acid (NODA) that can be labeled with ^{18}F using Al−F complex and examined their radiochemistries, in vitro and in vivo biological properties, and animal PET imaging characteristics. We found that the synthesized derivatives have excellent ^{18}F-labeling efficiencies, high stabilities, specific uptakes in cultured hypoxic tumor cells, and high tumor to nontumor ratios in xenografted mice. Furthermore, the derivatives were labeled with ^{18}F in a straightforward manner within 15 min at high labeling efficiencies and radiochemical purities. In conclusion, ^{18}F-labeled NODA−nitroimidazole conjugates were developed and proved to be promising hypoxia PET agents.

INTRODUCTION

Hypoxia is a characteristic of many tumors, especially solid tumors, due to oxygen deficiency caused by a poorly organized vasculature.[1,2] Tumor hypoxia is an important factor for the treatment of human cancers[3] because hypoxic cells are a major cause of radiation therapy and chemotherapy failure.[4,5] Many studies have been undertaken to develop accurate and practical means of quantifying hypoxia using noninvasive techniques. In particular, positron emission tomography (PET) has received much attention[6] because of its wide scope, high sensitivity, and because it allows hypoxia to be quantified.[7]

Nitroimidazoles undergo one-electron reduction by intracellular reductases in a reverse oxygen dependent manner to generate reactive intermediates that covalently bind to cellular constituents,[8] and this reduction may be useful in the context of designing hypoxia targeting and imaging strategies. In particular, the trapping of bioreductive substances in vivo indicates the presence of cellular hypoxia. However, the quantification of extent of hypoxia requires that nitroimidazole binding be primarily dependent on oxygen concentration in tumor cells.

The first nitroimidazole derivative used for imaging hypoxia was [^{18}F]fluoromisonidazole ([^{18}F]FMISO),[9,10] which was proposed as a potential tracer for determining tumor hypoxia in vivo by clinical PET in 1984. Subsequently, [^{18}F]-fluoroerythronitroimidazole ([^{18}F]FETNIM),[11] 1-*R*-D-(2-deoxy-2-[^{18}F]fluoroarabinofuranosyl)-2-nitroimidazole ([^{18}F]-FAZA),[12,13] 2-(2-nitro-1*H*-imidazol-1-yl)-*N*-(2,2,3,3,3-[^{18}F]-pentafluoropropyl) acetamide ([^{18}F]EF-5),[14] and 1-(3-[^{18}F]-fluorodialkylsilyl)propyl)-2-nitroimidazole[15] were developed as potential ^{18}F-labeled hypoxia imaging agents.

Received: November 29, 2011
Published: March 23, 2012

However, the preparations of all of these agents require multistep ^{18}F-labeling reactions such as repeated azeotropic evaporations, radiolabeling at high temperature in organic solvent containing base catalyst, purification by high performance liquid chromatography (HPLC), and the evaporation of organic solvents. The multiple evaporation steps required are particularly time-consuming and problematic with respect to automated preparation. In fact, various solvents and catalysts and new modalities, such as microfluidics, have been investigated to overcome these preparation problems.[16−19]

Recently, an innovative and straightforward labeling method that allows agents to be prepared within 15 min without an evaporation step was devised.[20−23] According to this method, ^{18}F incorporation is performed as a final step. Briefly, ^{18}F is first attached to aluminum to form Al^{18}F complex, which is then chelated to compounds like 1,4,7-triazacyclononane-1,4,7-triacetic acid (NOTA) preattached to a peptide or another molecule.

Herein, we present a labeling approach that takes advantage of this method. In the present study, we focused on the synthesis of AlF-1,4,7-triazacyclononane-1,4-diacetic acid (NODA)−nitroimidazole derivatives (Figure 1) and performed

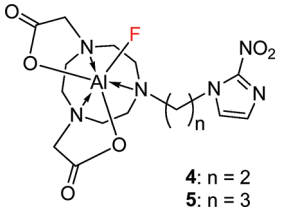

Figure 1. Proposed structures of aluminum fluoride complexes of nitroimidazole derivatives.

in vitro and in vivo studies on the labeled derivatives to determine their abilities to visualize hypoxia. Labeling NODA (a bifunctional ligand) was conducted using a rapid one-pot method. Labeling efficiencies were determined and PET and biodistribution studies were conducted.

RESULTS AND DISCUSSION

NOTA is a well-known cyclic chelating agent with three acetic acid side chains and forms a highly stable chelate with gallium.[24,25] Thus, various NOTA-based agents have been developed for labeling with ^{68}Ga.[26−32] Fluoride binds strongly to aluminum, which can also form a stable chelate with NOTA,[33,34] and thus several NOTA-based agents have been developed for labeling with ^{18}F using Al^{18}F complex.[20−22] Recently, it was reported that to achieve high ^{18}F-labeling efficiency of NOTA derivatives, electron donating atoms, such as nitrogen or oxygen, should not be present at positions that form pentagon or hexagon after bonding with aluminum.[35] Thus, NODA was chosen rather than NOTA because it lacks a carboxyl group that could interfere with ^{18}F binding by formation of pentagon ring after complexing with aluminum. In the present study, although the nitrogen atoms of the nitroimidazole residue in Al^{18}F-**4** and Al^{18}F-**5** are at positions that could form pentagon and hexagon, respectively, after bonding with aluminum, labeling efficiency was high because of the low reactivity of the nitrogen atoms by resonance stabilization and electron withdrawing nitro group.

To synthesize NODA−nitroimidazole conjugates, nitroimidazole was first reacted with 1,2-dibromoethane or 1,3-dibromopropane in DMF using K_2CO_3 as a base by stirring at room temperature overnight (Scheme 1). Pure **2** and **3** were

Scheme 1. Synthesis of NODA and the Nitroimidazole Conjugates[a]

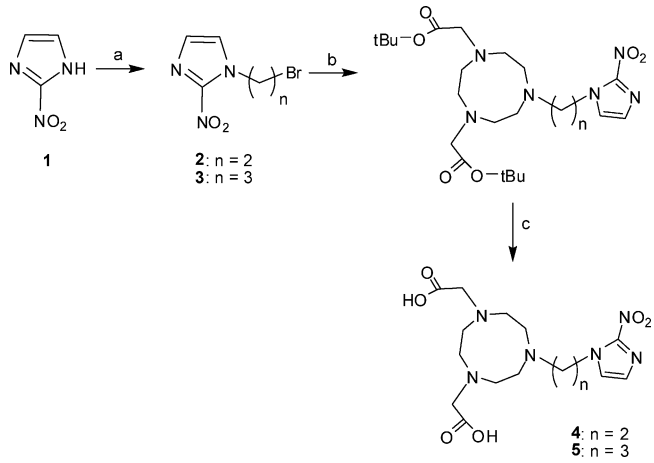

[a]Reagents and conditions for **4** and **5** synthesis: (a) $EtBr_2/PrBr_2$ (3.0 equiv), K_2CO_3 (0.5 equiv), DMF, rt; (b) NODA^{t}Bu (0.3 equiv), K_2CO_3 (1.0 equiv), MeCN, rt ; (c) HCl/dioxane, rt.

obtained by silica gel column purification and by recrystallization in ether, respectively, and these were then conjugated with NODA^{t}Bu in MeCN using K_2CO_3 as a base at room temperature (Scheme 1). After silica gel column purification, compounds **4** and **5** were obtained by removing the ^{t}Bu groups with concd HCl at room temperature. The compounds were purified by RP-HPLC after confirming reaction completion by mass spectroscopy. The chemical structures of the synthesized products were confirmed by NMR and mass spectroscopy. Their purities were checked by analytical HPLC, and NODA−nitroimidazole derivatives **4** and **5** exhibited a single peak.

To label **4** and **5** with ^{18}F, ^{18}F−Al complex was first prepared by mixing [^{18}F]fluoride and $AlCl_3$ stock solution in 0.1 M AcONa (pH 4) at room temperature. The prepared Al^{18}F was reacted with NODA−nitroimidazole derivatives, and labeling efficiencies were checked by ITLC-SG and found to be 84.5 ± 1.3% and 87.9 ± 2.7% for Al^{18}F-**4** and Al^{18}F-**5**, respectively (Figure 2). The radiochemical purities of both the derivatives after alumina N-cartridge purification were greater than 99% as determined by ITLC (Figure 2). The specific activities of Al^{18}F-**4** and Al^{18}F-**5** were 4.3 and 3.9 GBq/μmol, respectively.

Both labeled derivatives showed high in vitro stabilities up to 4 h in prepared medium at room temperature and in human serum at 37 °C. These stabilities in human serum also show that the labeled derivatives are stable in the presence of serum proteinases (Figure 3).

The serum protein binding activities of the radiolabeled derivatives were determined by incubation in fresh human serum at 37 °C. Al^{18}F-**4** exhibited protein-bound fractions of 0.24 ± 0.03% and 0.64 ± 0.03% after 10 and 60 min of incubation, respectively, and Al^{18}F-**5** had protein-bound fractions of 0.32 ± 0.06 and 0.36 ± 0.07%, respectively. These low protein binding levels are important for rapid uptake by target tissues and rapid clearance from blood and nontarget tissues.

In vitro cell uptake studies were conducted to determine the specific uptakes of Al^{18}F-**4** and Al^{18}F-**5** using HeLa, CHO, and

dx.doi.org/10.1021/jm201611a | J. Med. Chem. 2012, 55, 3155−3162

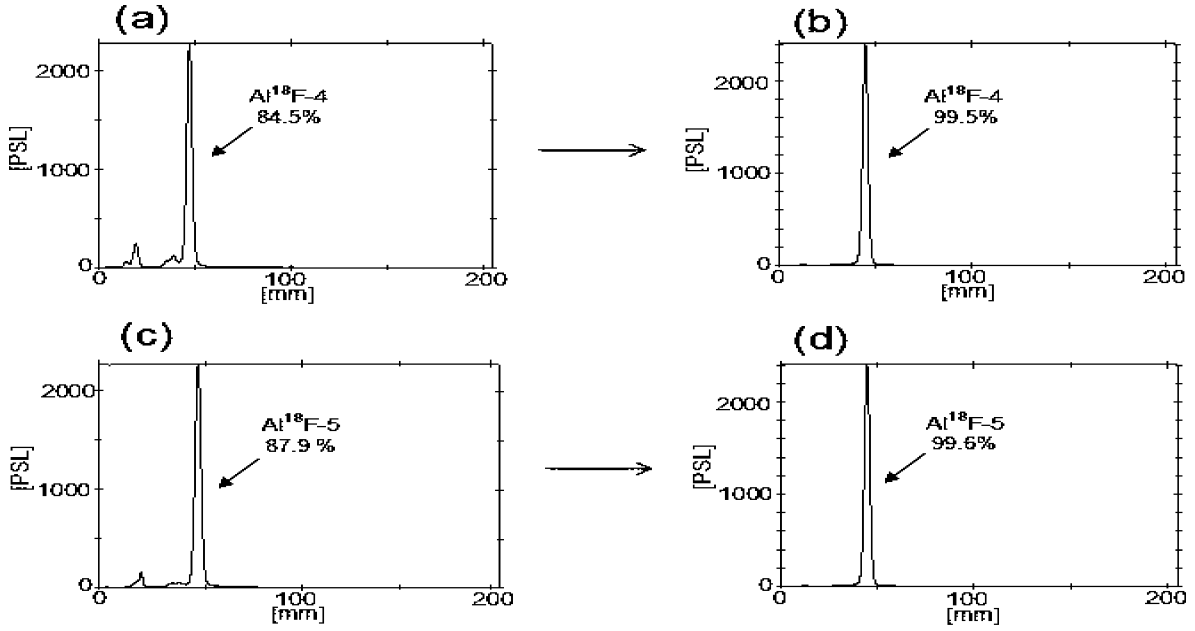

Figure 2. Radio-TLC of (a) crude $Al^{18}F$-**4**, (b) purified $Al^{18}F$-**4**, (c) crude $Al^{18}F$-**5**, and (d) purified $Al^{18}F$-**5**.

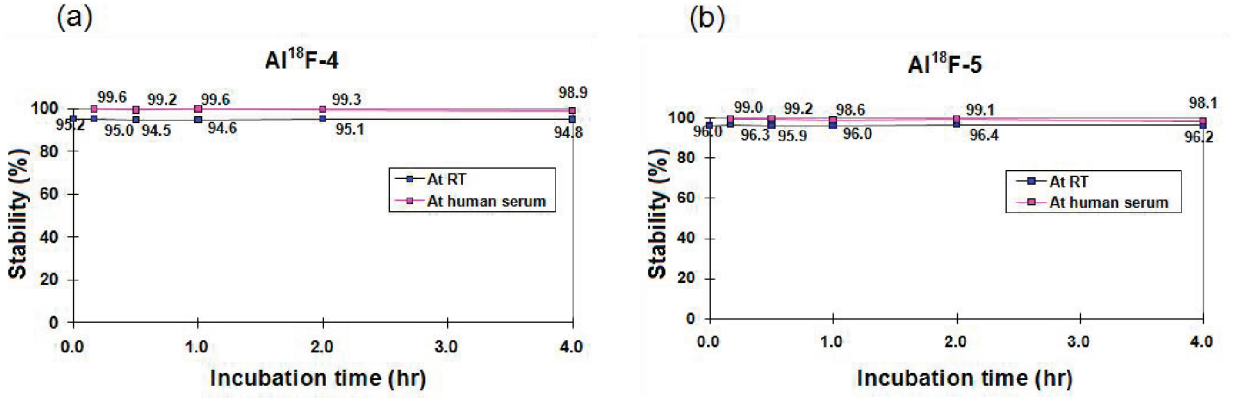

Figure 3. Stability studies of (a) $Al^{18}F$-**4** and of (b) $Al^{18}F$-**5** in prepared medium and in human serum.

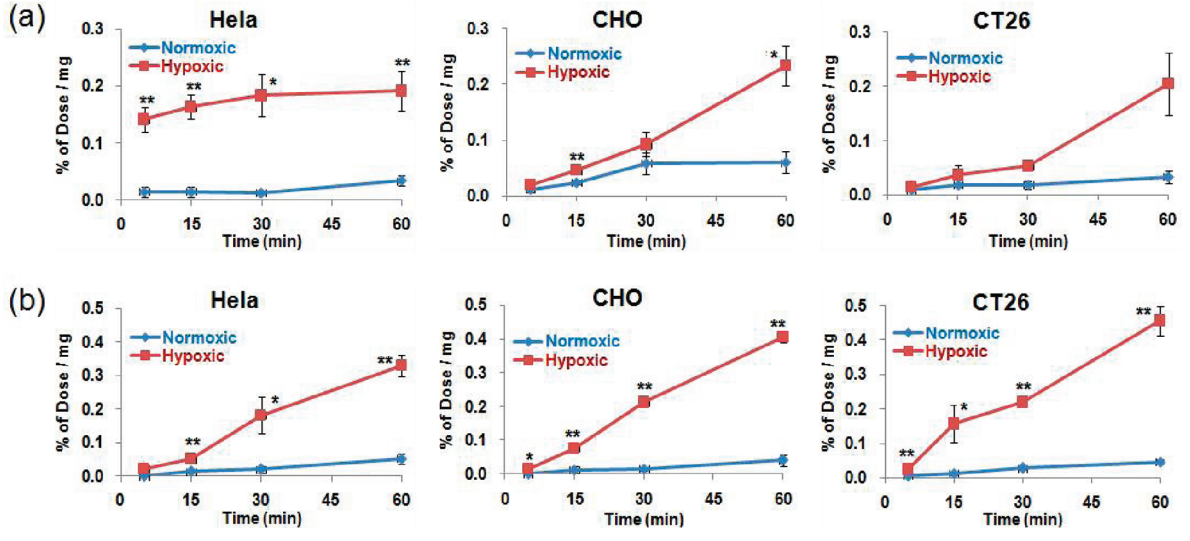

Figure 4. In vitro cell uptake studies for determination of the specific uptakes of the novel tracers (a) $Al^{18}F$-**4** and (b) $Al^{18}F$-**5** under normoxic and hypoxic conditions using HeLa, CHO, and CT-26 cells. *p* values are of comparisons between uptakes under normoxic and hypoxic conditions (*t* test): (**) $p < 0.01$, (*/) $p < 0.05$, $n = 4$ at each time point.

dx.doi.org/10.1021/jm201611a | J. Med. Chem. 2012, 55, 3155–3162

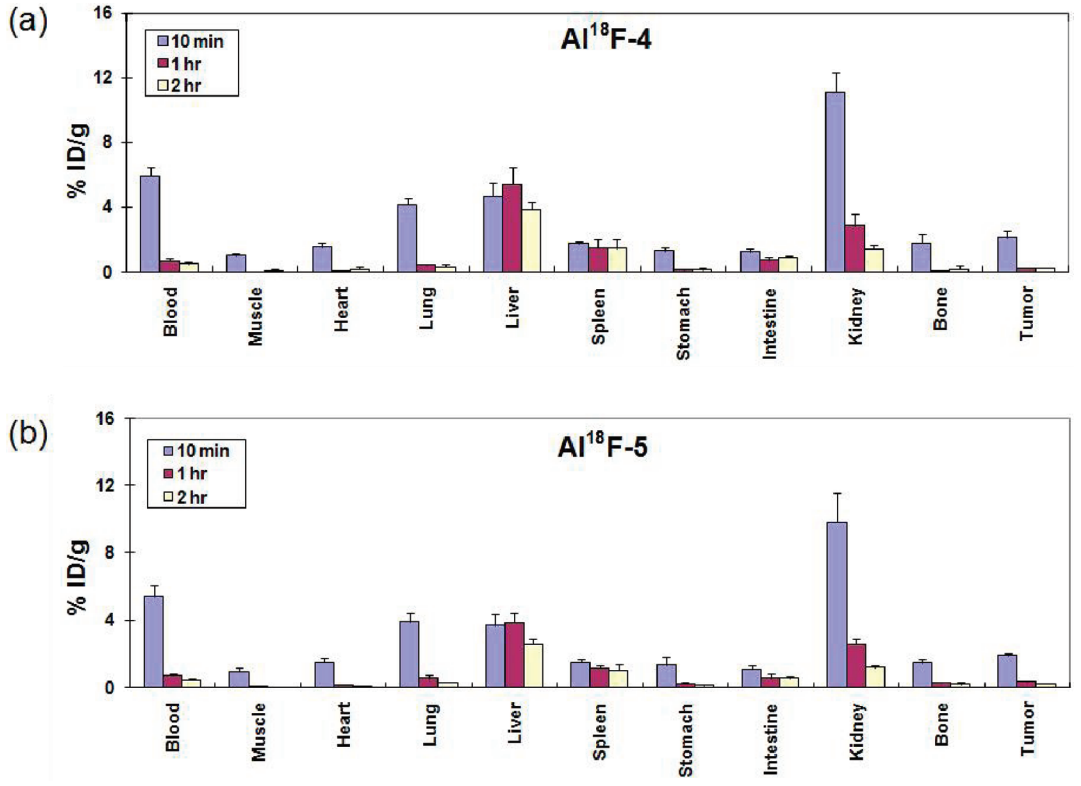

Figure 5. Biodistribution study at 10, 60, and 120 min postinjection for (a) $Al^{18}F$-**4** and (b) $Al^{18}F$-**5** in CT-26 xenografted mice. Results are mean percentage of injected dose per gram of tissue ± standard deviation (% ID/g ± SD); n = 4 at each time point.

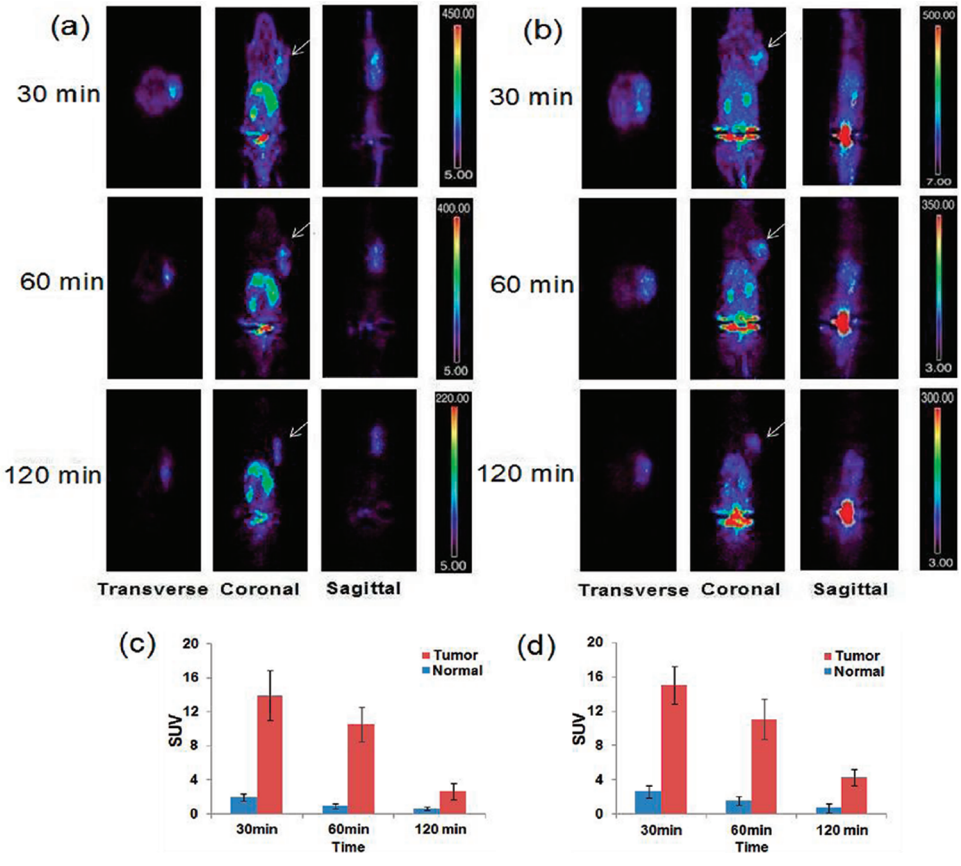

Figure 6. Representative microPET images of CT26 tumor bearing mice at 30, 60, and 120 min after intravenous injection of (a) $Al^{18}F$-**4** or (b) $Al^{18}F$-**5**. Arrows indicate tumors. (c,d) SUV of $Al^{18}F$-**4** and $Al^{18}F$-**5**, respectively.

dx.doi.org/10.1021/jm201611a | *J. Med. Chem.* 2012, 55, 3155–3162

CT-26 cell lines (Figure 4). All three cell lines showed elevated uptakes of $Al^{18}F$-**4** and $Al^{18}F$-**5** under the hypoxic versus the normoxic condition. Both derivatives demonstrated increasing uptake ratios from 5 to 60 min, except for $Al^{18}F$-**4** in HeLa cells, in which the hypoxic to normoxic uptake ratio of $Al^{18}F$-**4** decreased from 9.8 at 5 min to 5.6 at 1 h. On the other hand, this ratio increased from 1.7 at 5 min to 3.8 at 1 h in CHO cells and from 1.6 at 5 min to 6.1 at 1 h in CT-26 cells. In the case of $Al^{18}F$-**5**, uptake ratios in HeLa, CHO, and CT-26 cells increased from 2.1 at 5 min to 6.3 at 1 h, from 2.1 at 5 min to 10.0 at 1 h, and from 4.5 at 5 min to 10.0 at 1 h,[36] respectively. Furthermore, for $Al^{18}F$-**4**, the uptake ratios of HeLa, CHO, and CT-26 cells under hypoxic versus normoxic conditions at 1 h were 5.6, 3.9, and 6.2, respectively, and for $Al^{18}F$-**5** were 6.3, 10.0, and 10.1, respectively, that is, ratios were higher for $Al^{18}F$-**5**. All these in vitro results represent higher hypoxic to normoxic uptake ratios than reported results of [^{18}F]FMISO and [^{18}F]FAZA.[36] For example, the in vitro hypoxic to normoxic uptake ratios of [^{18}F]FMISO and [^{18}F]FAZA were shown as 1.5 and 1.4 at 10 min, respectively, and 3.0 and 2.7 at 100 min, respectively.[36]

A biodistribution study was performed using mouse colon cancer CT-26 xenografted balb/c mice (n = 4) after injecting $Al^{18}F$-**4** and $Al^{18}F$-**5** via a tail vein (Figure 5). Mice were sacrificed at 10, 60, and 120 min postinjection. At 10 min postinjection, the highest uptakes of both labeled derivatives were observed in kidneys, and this uptake decreased rapidly with time, indicating that the renal excretion route predominated. Liver, lung, and blood followed kidneys in terms of uptake levels for both derivatives at 10 min postinjection. Blood and lung activities rapidly decreased, whereas liver activity did not. $Al^{18}F$-**4** showed higher liver uptake than $Al^{18}F$-**5**, which was somewhat unlikely because $Al^{18}F$-**5** might be more lipophilic than $Al^{18}F$-**4**. Tumor uptakes at 10 min postinjection were 2.13 ± 0.41 and 1.92 ± 0.12% ID/g for $Al^{18}F$-**4** and $Al^{18}F$-**5**, respectively, and both decreased by time (at 60 min 0.24 ± 0.03% ID/g for $Al^{18}F$-**4** and 0.33 ± 0.05%ID/g for $Al^{18}F$-**5**, and at 120 min 0.23 ± 0.05% ID/g for $Al^{18}F$-**4** and 0.22 ± 0.04% ID/g for $Al^{18}F$-**5**). All other normal organs also showed decreasing activities. Highest tumor-to-muscle (T/M) and tumor to blood (T/B) ratios were 14.50 at 60 min and 0.49 at 120 min for $Al^{18}F$-**4** and 37.44 at 60 min and 0.50 at 120 min for $Al^{18}F$-**5** (Figure 5). According to the literature, T/B ratios of $Al^{18}F$-**4** (0.38) and $Al^{18}F$-**5** (0.45) were lower than [^{18}F]FMISO (1.19) and [^{18}F]FAZA (3.27) at 60 min.[36] However, T/B ratios of $Al^{18}F$-**4** (14.50) and $Al^{18}F$-**5** (3.87) were higher than [^{18}F]FMISO (1.65) and [^{18}F]FAZA (1.69) at 60 min.[36] These differences partly could be due to the lipophilicity differences of the agents. After intravenous injection, more lipophilic compounds can penetrate into tissues more rapidly and resulting in rapid blood concentration decrease, however, they will show higher and prolonged normal tissue uptakes.

Animal PET imaging studies were also conducted in mice (n = 3) bearing CT-26 xenografts (Figure 6). A small animal PET/CT scanner was used, and images were obtained at 30, 60, and 120 min postinjection. Tumors were visualized using labeled agents, and tumor uptakes were found to decrease with time (Figure 6). Both agents showed high kidney uptakes, however, liver uptake was higher for $Al^{18}F$-**4**, which concurs with our biodistribution study findings. SUVs and tumor to nontumor (T/N) ratios were calculated using PET data for quantitative analysis. T/N ratios for both labeled derivatives increased with time: at 30, 60, and 120 min, the T/N ratios of $Al^{18}F$-**4** were 7.2 ± 1.9, 11.5 ± 1.7, and 4.2 ± 0.8, and those of $Al^{18}F$-**5** were 5.8 ± 1.5, 7.1 ± 1.9, and 6.4 ± 0.4, respectively. These values were higher than literature values of [^{18}F]FMISO (2.7) and [^{18}F]FAZA (2.4) at 60 min.[36]

CONCLUSIONS

In conclusion, we describe the design and synthesis of NODA–nitroimidazole derivatives that can be labeled with ^{18}F in a straightforward manner within 15 min with high labeling efficiency and high radiochemical purity. The described aluminum fluoride method eliminates drying steps from the labeling procedure, which is a major advantage as compared with other ^{18}F-labeling methods. Furthermore, both of the labeled nitroimidazole derivatives were found to be stable in vitro and to exhibit low serum protein binding. In addition, comparative in vitro cell uptake studies under hypoxic and normoxic conditions demonstrated that both agents were preferentially taken up by hypoxic cancer cells. Our biodistribution study also showed the derivatives have high target to nontarget tissue ratios and that they are rapidly cleared from blood and nontarget tissues. Finally, our PET study findings suggest that $Al^{18}F$-NODA–nitroimidazole derivatives are promising agents for the detection of hypoxia. Synthesis of ^{18}F-labeled nitroimidazole compounds having smaller molecular weight and more hydrophilic nature might contribute to develop PET agents showing faster infiltration into hypoxic tumors, faster blood clearance, and lower normal tissue uptakes.

EXPERIMENTAL SECTION

General. Di-*tert*-butyl 1,4,7-triazacyclononane-1,4-diacetate (NODA^{t}Bu) was purchased from CheMatech (Dijon). HPLC grade MeCN was purchased from Fischer Scientific Korea (Seoul). All the other commercial chemicals were obtained from Sigma-Aldrich (St. Louis, MO) and were used as supplied. All reactions were performed under a nitrogen atmosphere. Thin layer chromatography (TLC) was carried out using precoated aluminum-backed silica gel 60 F_{254} TLC plates (Darmstadt) to verify product purities. Waters Sep-Pak Light Accell Plus QMA cartridges and alumina-N cartridges were from Waters (Milford, MA). Instant thin layer chromatography-silica gel (ITLC-SG) plates were purchased from Varian, Agilent Technologies (Lake Forest City, CA). PD-10 desalting columns were purchased from GE Healthcare (Buckinghamshire, UK).

Mass analysis was performed using a Waters ESI ion trap spectrometer with electrospray ionization (ESI) or using high resolution mass spectra (HRMS) obtained using a Jeol, JMS-600W Agilent 6890 series mass spectrometer (Tokyo, Japan) with fast atomic bombardment (FAB^+) ionization detection in positive ion mode. The samples were diluted 50 times with MeOH or MeCN and injected directly into the mass spectrometers. ^{1}H NMR and ^{13}C NMR spectra were recorded using an AL 300 FT NMR spectrometer (300 MHz for ^{1}H and 75 MHz for ^{13}C; Jeol, Tokyo). ^{1}H NMR chemical shifts are reported in parts per million (ppm) with respect to tetramethylsilane with solvent resonances of CD_3OD at 3.31 and 4.87 ppm. ^{13}C NMR spectra were recorded at 500 MHz with solvent resonance of CD_3OD at 49.1 ppm.

To purify the synthesized compounds, an XTerra prep RP18 10 μm (10 mm × 250 mm) column (Waters Co.) at a flow rate of 5 mL/min was used using solvent A (10 mM TFA in H_2O) and solvent B (MeCN). The HPLC UV detector was preset at 215 and 240 nm. Analytical reverse phase (RP)-HPLC was performed using an XTerra RP18 3.5 μm (4.6 mm × 100 mm) column (Waters Co.), using the same conditions at a flow rate of 1 mL/min. The purities of synthesized compounds were higher than 95% by analytical HPLC (Supporting Information Figure 11S and 22S).

The γ scintillation counter was from Packard Cobra II (Global Market Institute, MN).

Nitroimidazole-ethylbromide (2). Dimethylformamide (DMF, 0.2 mL) was added to a mixture of 2-nitroimidazole (**1**) (0.050 g, 0.44 mmol) and K_2CO_3 (0.031 g, 0.22 mmol) with stirring, and then 1,2-dibromoethane (0.249 g, 1.32 mmol) in DMF (0.5 mL) was added dropwise to the mixture again with stirring and left to stir at room temperature overnight. Reaction completion was confirmed by TLC. The mixture was then filtered, and the solid obtained was washed several times with MeOH. The solvent was then evaporated off, and the solid obtained was purified by column chromatography using EtOAc/hexane (2:8) to afford pure compound **2** as a yellow solid (0.085 g, 0.39 mmol, 84%). ^{1}H NMR (300 MHz, CD_3OD) δ: 7.23 (s, 1H), 7.09 (s, 1H), 4.77 (t, 2H), 3.70−3.72 (t, J = 6 Hz, 2H). ^{13}C NMR (75 MHz, CD_3OD) δ: 144.2, 128.0, 127.1, 50.1, 29.6. Mass spectrum (ESI$^+$), $(M)^+$ and $(M + 2H)^+$ calcd for $C_5H_7BrN_3O_2$, 219.97 and 221.97; found, 220.0 and 222.0. R_f = 0.6 (60% hexane, 40% EtOAc).

Nitroimidazole-propylbromide (3). K_2CO_3 (0.061 g, 0.44 mmol) was added to a stirring solution of **1** (0.100 g, 0.88 mmol) in DMF (0.5 mL). 1,3-Dibromopropane (0.536 g, 2.65 mmol) in DMF (1 mL) was then added dropwise, and the reaction mixture was stirred at room temperature overnight. Reaction completion was confirmed by TLC. The reaction mixture was then quenched with water and extracted with EtOAc. After removing the solvent in vacuo, ether was added to the residue and the mix was filtered. The solid obtained was washed with ether, and the filtrate was evaporated to obtain pure compound **3** as a yellow solid (0.180 g, 0.77 mmol, 88%). ^{1}H NMR (300 MHz, CD_3OD δ: 7.25 (s, 1H), 7.17 (s, 1H), 4.66−4.61 (t, J = 15 Hz, 2H), 3.43−3.39 (t, J = 12 Hz, 2H), 2.48-2.39 (m, 2H). ^{13}C NMR (75 MHz, CD_3OD) δ: 144.5, 128.5, 126.4, 48.1, 32.4, 29.0. Mass spectrum (ESI$^+$), $(M)^+$ and $(M + 2H)^+$ calcd for $C_6H_9BrN_3O_2$, 233.99 and 235.99; found, 234.0 and 236.0. R_f = 0.5 (70% hexane, 30% EtOAc).

NODA^{t}Bu−ethylnitroimidazole. A mixture of NODA^{t}Bu (0.050 g, 0.14 mmol) and K_2CO_3 (0.058 g, 0.42 mmol) was stirred in MeCN (2 mL). A solution of **2** (0.046 g, 0.42 mmol) in MeCN (1 mL) was then added dropwise to this mixture with vigorous stirring at room temperature, and the reaction mixture was left to stir for 20 h. Reaction completion was confirmed by TLC, and the mixture was filtered. The solid obtained was washed with MeCN, and the residual solvent was evaporated. The crude compound obtained was purified by column chromatography using MeOH/$MeCl_2$ (1:9) to produce pure solid (0.035 g, 0.71 mmol, 63%). ^{1}H NMR (300 MHz, CD_3OD) δ: 7.63 (s, 1H), 7.14 (s, 1H), 4.68 (t, 2H), 3.50−3.42 (m, 8H), 3.18 (s, 1H), 3.00−2.93 (m, 9H), 1.49−1.47 (m, 18H). ^{13}C NMR (75 MHz, CD_3OD) δ: 170.1, 144.3, 128.0, 127.3, 81.4, 58.0, 56.4, 53.2, 49.7, 47.1, 27.8. Mass spectrum (ESI$^+$), $(M + H)^+$ calcd for $C_{23}H_{41}N_6O_6$, 497.4; found, 497.4. R_f = 0.4 (95% $MeCl_2$, 5% MeOH).

NODA^{t}Bu−propylnitroimidazole. K_2CO_3 (0.058 g, 0.42 mmol) was added to a stirring solution of NODA^{t}Bu (0.050 g, 0.14 mmol) in MeCN (2 mL). Compound **3** (0.098 g, 0.42 mmol) in MeCN (1 mL) was then added dropwise, and the reaction mixture was stirred at room temperature for 20 h. Reaction completion was confirmed by TLC. The reaction mixture was then filtered, and the solid obtained was washed with MeCN. Solvent was evaporated, and the crude compound obtained was purified by column chromatography using MeOH/$MeCl_2$ (1:9) to afford pure compound as yellow solid (0.051 g, 0.99 mmol, 70%). ^{1}H NMR (300 MHz, CD_3OD δ: 7.37 (s, 1H), 7.05 (s, 1H), 4.53−4.49 (t, J = 12 Hz, 2H), 3.25 (s, 4H), 2.84−2.81 (m, 8H), 2.66−2.64 (m, 4H), 2.46−2.42 (t, 2H), 1.96−1.87 (m, 2H), 1.39 (s, 18H). ^{13}C NMR (75 MHz, CD_3OD) δ: 171.4, 144.7, 128.2, 127.2, 80.8, 59.7, 56.1, 55.8, 55.6, 54.6, 48.2, 28.4, 28.1. Mass spectrum (ESI$^+$), $(M + H)^+$ calcd for $C_{24}H_{43}N_6O_6$, 511.32; found, 511.2. R_f = 0.4 (95% $MeCl_2$, 5% MeOH).

NODA−ethylnitroimidazole (4). Concd HCl (0.5 mL) was added to a solution of NODA^{t}Bu−ethylnitroimidazole (0.026 g, 0.05 mmol) in dioxane (2 mL) and stirred vigorously at room temperature for 15 h. Product formation was confirmed by mass analysis. RP-HPLC (0−100% of B for 30 min and 100% of B for 5 min) was used to purify crude compound **4** to obtain the pure compound as a light-yellow solid (0.017 g, 0.44 mmol, 85%). Purity of the product obtained was confirmed using an analytical HPLC with the same conditions used for the purification. ^{1}H NMR (300 MHz, CD_3OD δ: 7.34 (s, 1H), 6.99 (s, 1H), 3.78 (s, 4H), 3.51 (s, 2H), 3.36 (s, 4H), 3.26 (s, 4H), 3.19 (s, 5H), 1.81 (s, 1H). ^{13}C NMR (75 MHz, CD_3OD) δ: 172.3, 145.0, 129.0, 128.8, 57.2, 55.7, 51.2, 50.9, 45.2. Mass spectrum (ESI$^+$), $(M + H)^+$ calcd for $C_{15}H_{25}N_6O_6$, 385.18; found, 385.3. HRMS (ESI$^+$), $(M + H)^+$ calcd for $C_{15}H_{25}N_6O_6$, 385.1836; found, 385.1837.

NODA−propylnitroimidazole (5). NODA^{t}Bu−propylnitroimidazole (0.024 g, 0.05 mmol) was dissolved in dioxane (2 mL) and concd HCl (0.5 mL) was then added and then stirred at room temperature for 15 h. Completion of reaction was cconfirmed by mass analysis. The resulting product was purified by RP-HPLC (50−90% of B for 30 min) to obtain pure compound **5** as a light-yellow solid (0.015 g, 0.38 mmol, 83%). Product purity was confirmed by analytical HPLC (using the same conditions as RP-HPLC) and by HRMS. ^{1}H NMR (300 MHz, CD_3OD) δ: 7.27 (s, 1H), 6.96 (s, 1H), 4.34 (brs, 2H), 3.75 (brs, 5H), 3.39−3.47 (m, 5H), 3.29 (brs, 4H), 3.16 (s, 4H), 2.23 (brs, 2H). ^{13}C NMR (75 MHz, CD_3OD) δ: 172.6, 144.8, 128.5, 128.4, 63.0, 57.2, 55.6, 51.6, 51.3, 50.3, 47.3, 25.3. Mass spectrum (ESI$^+$), $(M + H)^+$ calcd for $C_{16}H_{27}N_6O_6$, 399.2; found, 399.3. HRMS (ESI$^+$), $(M + H)^+$ calcd for $C_{16}H_{27}N_6O_6$, 399.1992; found, 399.1996.

AlF-4. $AlCl_3$ solution (0.416 mg, 3.12 μmol, 1.2 eq in 100 μL of water) was added to solution of **4** (1 mg, 2.60 μmol, 1.0 equiv in 100 μL of water) and adjusted to pH 3.5 using 1 M sodium acetate buffer. Reaction mixture was stirred for 30 min at 100 °C on water bath. NaF (0.546 mg, 13 μM, 5.0 equiv) was added to the reaction mixture and heated for 1 h. Completion of the reaction was checked by mass analysis and purified by RP-HPLC (0−100% of B for 30 min and 100% for 5 min) and lyophilized to afford pure complex as white solid. HRMS (ESI$^+$), $(M + Na)^+$: calcd, 451.1298; observed, 451.1292.

AlF-5. $AlCl_3$ (13.3 mg, 0.1 mmol) was added to solution of **5** (35 mg, 0.09 mmol in 2 mL water) and the pH of the reaction mixture was adjusted to 4.4 using 1 M sodium acetate buffer and boiled for an hour. Sodium fluoride was added to the reaction mixture and boiling continued for one more hour. Completion of the reaction was checked by mass analysis and purified by RP-HPLC (0−100% of B for 30 min and 100% for 5 min) and lyophilized to afford pure complex as white solid. HRMS (ESI$^+$), $(M + H)^+$: calcd, 443.1635; observed, 443.1630.

Radionuclide Labeling. ^{18}F was produced using the ^{18}O (p,n) ^{18}F reaction using ^{18}O-enriched (95%) water produced using a cyclotron, CYCLONE 18/9 (IBA, Ion Beam Applications, Louvain-la-Neuve, Belgium). ^{18}F in water was loaded onto a QMA cartridge (prewashed with 5 mL of 0.4 M $KHCO_3$ and 10 mL of water), washed with water (5 mL), and then eluted with 0.4 mL of normal saline. Glacial acetic acid (4 μL) was then added to adjust pH of the ^{18}F solution to 4. Separately, a stock solution of 2 mM $AlCl_3$ was prepared by dissolving $AlCl_3{\cdot}6H_2O$ in 0.1 M AcONa buffer (pH 4). Al^{18}F was prepared by mixing 45 nmol stock $AlCl_3$ solutions (22.5 μL) with the eluted ^{18}F saline solution (50 μL, 66.6−115.8 MBq) and incubating the mix at room temperature for 10 min. The prepared Al^{18}F solution was added to solution of synthesized ligands (50 nmol) in 0.1 M sodium acetate buffer (1 mL). Reaction mixture was placed on 110 °C heating block for 10 min. Labeled compounds were passed through an Alumina-N light cartridge (prewashed with 5 mL of normal saline) to remove unlabeled Al^{18}F and washed with normal saline (3 mL). The labeled products were analyzed by HPLC using XBridge Prep C18 column (10 mm × 250 mm, Waters Co., USA) eluted with programmed solvent (0.01 M HCl; EtOH increased from 0% to 50% for 30 min at 2 mL/min) and no impurity was found (Supporting Information Figure 23S and 24S).

Stability Study. The stabilities of Al^{18}F-NODA−nitroimidazole derivatives in the prepared medium at room temperature and in human serum at 37 °C were determined by ITLC-SG (80% MeCN in water).

Serum Protein Binding by Al^{18}F-NODA−nitroimidazole Derivatives. Serum protein binding fractions were determined as previously described.[25,28] Briefly, PD-10 columns were preconditioned by loading them with 1.0 mL of 1% bovine serum albumin in 0.1 M DTPA and repeated washing with 100 mL of phosphate buffered saline (PBS). Al^{18}F-NODA−nitroimidazole derivatives (1.5 MBq/10 μL) were mixed with human serum (1 mL) and incubated for 10 or 60

min at 37 °C. Each mixture was loaded onto a preconditioned PD-10 column and eluted with PBS; 30 fractions (fraction size 0.5 mL) were collected per sample in 5 mL test tubes. Fraction radioactivities were measured using a γ counter and expressed as cpm (counts per minute). To check for the presence of protein in each fraction, aliquots (2 μL) from each test tube were spotted on a filter paper and stained with Coomassie blue. Protein bound fractions were appeared at the void volume and free fractions at the bed volume.

In Vitro Cell Uptake Study. A Chinese hamster ovarian cancer cell line (CHO), a Henrietta Lacks cervical cancer cell line (HeLa), and a mouse colon cancer cell line (CT26) were supplied by the Korean Cell Line Bank (KCLB, Seoul). All cell lines were maintained in Dulbecco's Modified Eagle's medium (DMEM) supplemented with 10% fetal bovine serum (both from Welgene Inc., Daegu) containing 1% antibiotics mixture (penicillin, streptomycin, and amphotericin B: 10000 IU/10 mg/25 μg/mL, Mediatech Inc. Manassas, VA). Cultures were maintained at 37 °C. Cells were subcultured overnight in 12-multiwell culture plates (4×10^5 cells/mL for each cell line) and preincubated under normoxic (5% CO_2 in air) or hypoxic (5% CO_2 in N_2) conditions for 4 h. Al^{18}F-**4** (0.18 MBq/100 μL) or Al^{18}F-**5** (0.18 MBq/100 μL) was added to wells and incubated for 5 or 60 min. Wells were then washed with DMEM, and cells were dissolved in 0.5% of sodium dodecyl sulfate (SDS) in PBS (0.5 mL). Tracer uptakes were measured using a γ counter, and total protein concentrations in samples were determined using the bicinchoninic acid method (Pierce, Rockford, IL).

Biodistribution Study in Mice Bearing Colon Cancer Xenografts. All animal experiments in mice were conducted using protocols approved by the Institutional Animal Care and Use Committee of the Clinical Research Institute at Seoul National University Hospital (an Association for the Assessment and Accreditation of Laboratory Animal Care-accreditated facility). In addition, National Research Council Guidelines for the Care and Use of Laboratory Animals (revised in 1996) were observed throughout. The mouse colon cancer cell line CT26 was grown in RPMI 1640 medium containing 10% fetal bovine serum and 1% antibiotics. CT26 cells were washed with 10 mL of PBS by centrifugation (3000 rpm). To induce tumor xenografts, CT26 cells were subcutaneously injected at a concentration of 4×10^5/ 0.1 mL into the right shoulders of each balb/c mice. At 14 days after tumor transplantation, all mice had developed a solid tumor mass (tumor weight 0.8−1.1 g). For biodistribution studies, each xenografted mouse (n = 4) was administered a labeled NODA−nitroimidazole agents (0.15 MBq/0.1 mL) through a tail vein. Mice were sacrificed by decapitation at 10, 60, and 120 min after radiotracer administration. Tumor, muscle, and major organs were excised, blotted, and weighed, and blood samples were taken; counts were obtained using a γ counter. The radioactivity contents of representative organs were expressed as percentages of injected dose per gram of tissue (% ID/g). Results are quoted as means and SDs for four animals.

Small Animal PET Studies. To compare in vivo uptake characteristics in CT26 bearing mice, PET studies were carried out using a dedicated small animal PET/CT scanner (GE Healthcare, Princeton, NJ). This unit contains hardware to control gantry and table motion and acquires image data using 36 detectors at an axial field of view (FOV) of 4.6 cm. Whole-body PET data were acquired in two bed positions and sorted into 20 frames (30 s per frames). Images were reconstructed by Fourier rebinning and by using the ordered subsets-expectation maximization (OSEM) reconstruction algorithm, using a ramp filter and the Nyquist limit (0.5 cycles/voxel) as the cutoff frequency without attenuation correction. CT26 cells (2×10^5 cells) in normal saline (0.1 mL) were subcutaneously injected into the mice right shoulders and grown for 14 days to produce tumors of diameter of ~16 mm. Al^{18}F-**4** (14.4 MBq/0.1 mL) or Al^{18}F-**5** (13.0 MBq/0.1 mL) was then intravenously injected through a tail vein. Mice were anesthetized with 2% isoflurane at 30, 60, and 120 min postinjection and placed near the center of the FOV of the microPET to maximize image resolution and sensitivity, and PET images were then obtained.

Data Analysis. ASIPro VM 5.0 software (Concorde Inc., Knoxville, TN) was used to process images. To assess the tumor uptakes of labeled derivatives, circular regions of interest (ROI) were placed (1.5 mm radius) at locations of maximum tracer uptake in tumors and in muscle (reference). Relative tracer uptakes are expressed as ratios of tumor versus muscle counts. Having placed ROIs, SUVs were calculated using, SUV = CCF/(injected dose/body weight), and CCF (decay corrected activity concentration) was calculated using, CCF (MBq/cc) = radioactivity (mCi/cc) × branching ratio × ROI (value/pixel); the branching ratio of ^{18}F is 0.967.

■ ASSOCIATED CONTENT

Ⓢ Supporting Information

MS (ESI+), HRMS, ^{3}H, and ^{13}C NMR spectra of the compounds and HPLC profiles of the ^{18}F-labeled compounds. This material is available free of charge via the Internet at http://pubs.acs.org.

■ AUTHOR INFORMATION

Corresponding Author

*Phone: +82-2-2072-3805. Fax: +82-2-745-7690. E-mail: jmjng@snu.ac.kr.

Notes

The authors declare no competing financial interest.

■ ACKNOWLEDGMENTS

This research was partly supported by the Converging Research Center Program (2010K001055) and National Research Laboratory Program (R0A-2008-000-20116-0) through the Ministry of Education, Sciences and Technology.

■ ABBREVIATIONS USED

PET, positron emission tomography; FMISO, fluoromisonidazole; FETNIM, fluoroerythronitroimidazole; FAZA, 1-*R*-D-(2-deoxy-2-fluoroarabinofuranosyl)-2-nitroimidazole; EF-5, 2-(2-nitro-1*H*-imidazol-1-yl)-*N*-(2,2,3,3,3-pentafluoropropyl) acetamide; HPLC, high performance liquid chromatography; NOTA, 1,4,7-triazacyclononane-1,4,7-triacetic acid; NODA, 1,4,7-triazacyclononane-1,4-diacetic acid; NMR, nuclear magnetic resonance; ITLC-SG, instant thin layer chromatography-silica gel; ID, injected dose; T/M, tumor-to-muscle; T/B, tumor-to-blood; SUV, standard uptake value; T/N, tumor-to-nontumor; ESI, electrospray ionization; HRMS, high resolution mass spetra; DTPA, diethylenetrimainepentaacetic acid; SDS, sodium dodecyl sulfate; FOV, field of view; OSEM, ordered subsets-expectation maximization; ROI, region of interest

■ REFERENCES

(1) Esteban, M. A.; Maxwell, P. H. HIF, a missing link between metabolism and cancer. *Nature Med.* **2005**, *11*, 1047−1048.

(2) Overgaard, J. Clinical evaluation of nitroimidazoles as modifiers of hypoxia in solid tumors. *Oncol. Res.* **1994**, *6*, 509−518.

(3) He, F.; Deng, X.; Wen, B.; Liu, Y.; Sun, X.; Xing, L.; Minami, A.; Huang, Y.; Chen, Q.; Zanzonico, P. B.; Ling, C. C.; Li, G. C. Noninvasive molecular imaging of hypoxia in human xenografts: comparing hypoxia-induced gene expression with endogenous and exogenous hypoxia markers. *Cancer Res.* **2008**, *68*, 8597−8606.

(4) Rofstad, E. K.; Sundfor, K.; Lyng, H.; Trope, C. G. Hypoxia-induced treatment failure in advanced squamous cell carcinoma of the uterine cervix is primarily due to hypoxia-induced radiation resistance rather than hypoxia-induced metastasis. *Br. J. Cancer* **2000**, *83*, 354−359.

(5) Nordsmark, M.; Overgaard, M.; Overgaard, J. Pretreatment oxygenation predicts radiation response in advanced squamous cell carcinoma of the head and neck. *Radiother. Oncol.* **1996**, *41*, 31−39.
(6) Lehtio, K.; Eskola, O.; Viljanen, T.; Oikonen, V.; Gronroos, T.; Sillanmaki, L.; Grenman, R.; Minn, H. Imaging perfusion and hypoxia with PET to predict radiotherapy response in head-and-neck cancer. *Int. J. Radiat. Oncol., Biol., Phys.* **2004**, *59*, 971−982.
(7) Rajendran, J. G.; Schwartz, D. L.; O'Sullivan, J.; Peterson, L. M.; Ng, P.; Scharnhorst, J.; Grierson, J. R.; Krohn, K. A. Tumor hypoxia imaging with [F-18] fluoromisonidazole positron emission tomography in head and neck cancer. *Clin. Cancer Res.* **2006**, *12*, 5435−5441.
(8) Whitmore, G. F.; Varghese, A. J. The biological properties of reduced nitroheterocyclics and possible underlying biochemical mechanisms. *Biochem. Pharmacol.* **1986**, *35*, 97−103.
(9) Tang, G.; Wang, M.; Tang, X.; Gan, M.; Luo, L. Fully automated one-pot synthesis of [^{18}F]fluoromisonidazole. *Nucl. Med. Biol.* **2005**, *32*, 553−558.
(10) Dubois, L.; Landuyt, W.; Haustermans, K.; Dupont, P.; Bormans, G.; Vermaelen, P.; Flamen, P.; Verbeken, E.; Mortelmans, L. Evaluation of hypoxia in an experimental rat tumour model by [^{18}F]fluoromisonidazole PET and immunohistochemistry. *Br. J. Cancer* **2004**, *91*, 1947−1954.
(11) Gronroos, T.; Bentzen, L.; Marjamaki, P.; Murata, R.; Horsman, M. R.; Keiding, S.; Eskola, O.; Haaparanta, M.; Minn, H.; Solin, O. Comparison of the biodistribution of two hypoxia markers [^{18}F]-FETNIM and [^{18}F]FMISO in an experimental mammary carcinoma. *Eur. J. Nucl. Med. Mol. Imaging* **2004**, *31*, 513−520.
(12) Piert, M.; Machulla, H. J.; Picchio, M.; Reischl, G.; Ziegler, S.; Kumar, P.; Wester, H. J.; Beck, R.; McEwan, A. J.; Wiebe, L. I.; Schwaiger, M. Hypoxia-specific tumor imaging with 18F-fluoroazomycin arabinoside. *J. Nucl. Med.* **2005**, *46*, 106−113.
(13) Beck, R.; Roper, B.; Carlsen, J. M.; Huisman, M. C.; Lebschi, J. A.; Andratschke, N.; Picchio, M.; Souvatzoglou, M.; Machulla, H. J.; Piert, M. Pretreatment ^{18}F-FAZA PET predicts success of hypoxia-directed radiochemotherapy using tirapazamine. *J. Nucl. Med.* **2007**, *48*, 973−980.
(14) Komar, G.; Seppanen, M.; Eskola, O.; Lindholm, P.; Gronroos, T. J.; Forsback, S.; Sipila, H.; Evans, S. M.; Solin, O.; Minn, H. ^{18}F-EF5: a new PET tracer for imaging hypoxia in head and neck cancer. *J. Nucl. Med.* **2008**, *49*, 1944−1951.
(15) Bohn, P.; Deyine, A.; Azzouz, R.; Bailly, L.; Fiol-Petit, C.; Bischoff, L.; Fruit, C.; Marsais, F.; Vera, P. Design of silicon-based misonidazole analogues and ^{18}F-radiolabelling. *Nucl. Med. Biol.* **2009**, *36*, 895−905.
(16) Kim, D. W.; Choe, Y. S.; Chi, D. Y. A new nucleophilic fluorine-18 labeling method for aliphatic mesylates: reaction in ionic liquids shows tolerance for water. *Nucl. Med. Biol.* **2003**, *30*, 345−350.
(17) Kim, H. W.; Jeong, J. M.; Lee, Y. S.; Chi, D. Y.; Chung, K. H.; Lee, D. S.; Chung, J. K.; Lee, M. C. Rapid synthesis of [F-18]FDG without an evaporation step using an ionic liquid. *Appl. Radiat. Isot.* **2004**, *61*, 1241−1246.
(18) Aerts, J.; Voccia, S.; Lemaire, C.; Giacomelli, F.; Goblet, D.; Thonon, D.; Plenevaux, A.; Warnock, G.; Luxen, A. Fast production of highly concentrated reactive [^{18}F] fluoride for aliphatic and aromatic nucleophilic radiolabelling. *Tetrahedron Lett.* **2010**, *51*, 64−66.
(19) Yang, B. Y.; Jeong, J. M.; Lee, Y. S.; Lee, D. S.; Chung, J. K.; Lee, M. C. Facile calculation of specific rate constants and activation energies of ^{18}F-fluorination reaction using combined processes of coat-capture-elution and microfluidics. *Tetrahedron* **2011**, *67*, 2427−2433.
(20) McBride, W. J.; Sharkey, R. M.; Karacay, H.; D'Souza, C. A.; Rossi, E. A.; Laverman, P.; Chang, C. H.; Boerman, O. C.; Goldenberg, D. M. A Novel Method of F-18 Radiolabeling for PET. *J. Nucl. Med.* **2009**, *50*, 991−998.
(21) Laverman, P.; McBride, W. J.; Sharkey, R. M.; Eek, A.; Joosten, L.; Oyen, W. J. G.; Chang, C. H.; Boerman, O. C; Goldenberg, D. M. A Novel Facile Method of Labeling Octreotide with F-18-Fluorine. *J. Nucl. Med.* **2010**, *51*, 454−461.
(22) McBride, W. J.; D'Souza, C. A.; Sharkey, R. M.; Karacay, H.; Rossi, E. A.; Chang, C. H.; Goldenberg, D. M. Improved ^{18}F labeling of peptides with a fluoride-aluminum-chelate complex. *Bioconjugate Chem.* **2010**, *21*, 1331−1340.
(23) D'Souza, C. A.; McBride, W. J.; Sharkey, R. M.; Todaro, L. J.; Goldenberg, D. M. High-Yielding Aqueous ^{18}F-Labeling of Peptides via Al^{18}F Chelation. *Bioconjugate Chem.* **2011**, *22*, 1793−1803.
(24) Jeong, J. M.; Kim, Y. J.; Lee, Y. S.; Lee, D. S.; Chung, J. K.; Lee, M. C. Radiolabeling of NOTA and DOTA with positron emitting ^{68}Ga and investigation of in vitro properties. *Nucl. Med. Mol. Imaging* **2009**, *43*, 330−336.
(25) Hoigebazar, L.; Jeong, J. M.; Choi, S. Y.; Choi, J. Y.; Shetty, D.; Lee, Y. S.; Lee, D. S.; Chung, J. K.; Lee, M. C.; Chung, Y. K. Synthesis and Characterization of Nitroimidazole Derivatives for ^{68}Ga-Labeling and Testing in Tumor Xenografted Mice. *J. Med. Chem.* **2010**, *53*, 6378−6385.
(26) Parker, D. Tumor Targeting with Radiolabeled Macrocycle Antibody Conjugates. *Chem. Soc. Rev.* **1990**, *19*, 271−291.
(27) Jeong, J. M.; Hong, M. K.; Chang, Y. S.; Lee, Y. S.; Kim, Y. J.; Cheon, G. J.; Lee, D. S.; Chung, J. K.; Lee, M. C. Preparation of a promising angiogenesis PET imaging agent: Ga-68-labeled c-(RGDyK)-isothiocyanatobenzyl-1,4,7-triazacyclononane-1,4,7-triacetic acid and feasibility studies in mice. *J. Nucl. Med.* **2008**, *49*, 830−836.
(28) Yang, B. Y.; Jeong, J. M.; Kim, Y. J.; Choi, J. Y.; Lee, Y. S.; Lee, D. S.; Chung, J. K.; Lee, M. C. Formulation of ^{68}Ga BAPEN kit for myocardial positron emission tomography imaging and biodistribution study. *Nucl. Med. Biol.* **2010**, *37*, 149−155.
(29) Hoigebazar, L.; Jeong, J. M.; Hong, M. K.; Kim, Y. J.; Lee, J. Y.; Shetty, D.; Lee, Y. S.; Lee, D. S.; Chung, J. K.; Lee, M. C. Synthesis of ^{68}Ga-labeled DOTA-nitroimidazole derivatives and their feasibilities as hypoxia imaging PET tracers. *Bioorg. Med. Chem.* **2011**, *19*, 2176−2181.
(30) Choi, J. Y.; Jeong, J. M.; Yoo, B. C.; Kim, K.; Kim, Y.; Yang, B. Y.; Lee, Y. S.; Lee, D. S.; Chung, J. K.; Lee, M. C. Development of ^{68}Ga-labeled mannosylated human serum albumin (MSA) as a lymph node imaging agent for positron emission tomography. *Nucl. Med. Biol.* **2011**, *38*, 371−379.
(31) Shetty, D.; Jeong, J. M.; Ju, C. H.; Kim, Y. J.; Lee, J. Y.; Lee, Y. S.; Lee, D. S.; Chung, J. K.; Lee, M. C. Synthesis and evaluation of macrocyclic amino acid derivatives for tumor imaging by gallium-68 positron emission tomography. *Bioorg. Med. Chem.* **2010**, *18*, 7338−7347.
(32) Shetty, D.; Jeong, J. M.; Ju, C. H.; Lee, Y. S.; Jeong, S. Y.; Choi, J. Y.; Yang, B. Y.; Lee, D. S.; Chung, J. K.; Lee, M. C. Synthesis of novel ^{68}Ga-labeled amino acid derivatives for positron emission tomography of cancer cells. *Nucl. Med. Biol.* **2010**, *37*, 893−902.
(33) Martin, R. Fe^{3+} and Al^{3+} hydrolysis equilibria. Cooperativity in Al^{3+} hydrolysis reactions. *J. Inorg. Biochem.* **1991**, *44*, 141−147.
(34) Martin, B. Ternary complexes of Al^{3+} and F^- with a third ligand. *Coord. Chem. Rev.* **1996**, *149*, 23−32.
(35) Shetty, D.; Choi, S. Y.; Jeong, J. M.; Lee, J. Y.; Hoigebazar, L.; Lee, Y. S.; Lee, D. S.; Chung, J. K.; Lee, M. C.; Chung, Y. K. Stable aluminium fluoride chelates with triazacyclononane derivatives proved by X-ray crystallography and ^{18}F-labeling study. *Chem. Commun.* **2011**, *47*, 9732−9734.
(36) Sorger, D.; Patt, M.; Kumar, P.; Wiebe, L. I.; Barthel, H.; Seese, A.; Dannenberg, C.; Tannapfel, A.; Kluge, R.; Sabri, S. [^{18}F]-Fluoroazomycinarabinofuranoside (^{18}FAZA) and [^{18}F]-fluoromisonidazole (^{18}FMISO): a comparative study of their selective uptake in hypoxic cells and PET imaging in experimental rat tumors. *Nucl. Med. Biol.* **2003**, *30*, 317−326.